PHYSICAL REVIEW B **96**, 241302(R) (2017)

High-resolution imaging of silicene on an Ag(111) surface by atomic force microscopy

Jo Onoda,[1,2,*] Keisuke Yabuoshi,[1] Hiroki Miyazaki,[1] and Yoshiaki Sugimoto[1,2]

[1]*Graduate School of Frontier Sciences, University of Tokyo, 5-1-5 Kashiwanoha, Kashiwa, Chiba 277-8561, Japan*

[2]*Graduate School of Engineering, Osaka University, 2-1 Yamada-Oka, Suita, Osaka 565-0871, Japan*

(Received 21 September 2017; revised manuscript received 16 November 2017; published 11 December 2017)

Silicene, a two-dimensional (2D) honeycomb arrangement of Si atoms, is expected to have better electronic properties than graphene and has been mostly synthesized on Ag surfaces. Although scanning tunneling microscopy (STM) has been used for visualizing its atomic structure in real space, the interpretation of STM contrast is not straightforward and only the topmost Si atoms were observed on the (4×4) silicene/Ag(111) surface. Here, we demonstrate that high-resolution atomic force microscopy (AFM) can resolve all constituent Si atoms in the buckled honeycomb arrangement of the (4×4) silicene. Site-specific force spectroscopy attributes the origin of the high-resolution AFM images to chemical bonds between the AFM probe apex and the individual Si atoms on the (4×4) silicene. A detailed analysis of the geometric parameters suggests that the pulling up of lower-buckled Si atoms by the AFM tip could be a key for high-resolution AFM, implying a weakening of the Si-Ag interactions at the interface. We expect that high-resolution AFM will also unveil atomic structures of edges and defects of silicene, or other emerging 2D materials.

DOI: 10.1103/PhysRevB.96.241302

Silicene, a Si analog of graphene forming a two-dimensional (2D) honeycomb structure, has attracted increasing attention for the past few years. Compared with graphene, silicene has a buckled structure along with stronger spin-orbit coupling strength. Therefore, a quantum-spin Hall effect at experimentally accessible temperatures and the tunability of the band gap by external fields has been anticipated [1]. Despite the intriguing electronic properties, we had to wait until 2012 for a breakthrough in the experimental synthesis of silicene [2,3]. The most common substrate for the preparation of single-monolayer silicene is the Ag(111) surface. Depending on the Si coverage and substrate temperature during growth, silicene can form a variety of commensurate superstructures relative to the substrate, such as (4×4) [2–11], $(\sqrt{13} \times \sqrt{13})R \pm 13.9^\circ$ [3–6,10,12–16], $(2\sqrt{3} \times 2\sqrt{3})$ [5–7,16–21], and $(4/\sqrt{3} \times 4/\sqrt{3})$ [4,10,15–17,22–25]. Regarding the controversy on the electronic structure of the (4×4) phase, it has been suggested that the Dirac cones do not survive at the K points of the silicene (1×1) Brillouin zone due to the strong interaction between silicene and the Ag(111) substrate [26]. On the other hand, Feng *et al.* recently reported the surprising finding of six pairs of Dirac cones at the edges of the first Brillouin zone of Ag(111) [27]. Thus, it remains open for debate whether silicene deposited on an Ag(111) surface could be a material that harnesses unique massless Dirac fermions.

To better understand the electronic structure of the above various phases, we must properly understand the geometric structures of silicene. So far, the atomic structure of silicene has been mainly characterized by low-energy electron diffraction (LEED) or scanning tunneling microscopy (STM). Although STM in particular allows real-space imaging of silicene at atomic resolutions, the contrast is mainly dominated by the electronic structure at around the Fermi level and/or subtle differences in the topographic heights; thus there is ambiguity in the interpretation of the obtained images. On the other hand, over the past decade, noncontact atomic force microscopy (AFM) has been established as an extremely powerful and versatile tool for structure analyses. Especially fascinating are recent observations of the chemical structure of various organic molecules with CO-functionalized tips [28]. While high-resolution AFM has begun to be applied to the surfaces of various 2D materials [29–32], few AFM studies of silicene using qPlus sensors [10,11] have been reported to date. The information regarding the geometric structure of silicene given by the AFM studies is comparable with that acquired by a previous STM study [2].

Here, we report an AFM observation of honeycomb structures of silicene grown on Ag(111). We found that AFM equipped with Si cantilevers can resolve the upper- and lower-buckled Si atoms in the (4×4) silicene sheet, the latter of which were not accessible in previous STM and AFM studies. The high-resolution AFM images enable us to discuss the geometric structures of silicene. We also carry out force spectroscopy measurements, with the result that the origin of the high-resolution AFM images is attributed to the chemical bond between the tip apex atom and the surface Si atoms of the (4×4) silicene on Ag(111).

All experiments were carried out using a custom-built frequency-modulation AFM at room temperature (RT) in ultrahigh vacuum (UHV; base pressure 5×10^{-9} Pa). We used commercial Pt-coated or uncoated Si cantilevers whose apices were cleaned by Ar^+ sputtering for the removal of native oxides. Our system is based on an optical fiber interferometer for detecting the oscillation of the cantilevers, which are mechanically excited. The voltage corresponding to the contact potential difference between the tip and sample was applied to the sample to minimize the effect of long-range electrostatic force. More details are described elsewhere [33]. Clean Ag(111) was prepared by repeated Ar^+ sputtering (2 keV, 1×10^{-3} Pa for 20 min) and annealing (600 °C) in UHV. The Si source for preparing silicene consisted of an Si wafer ($10 \times 3 \times 0.5$ mm^3) subjected to resistive heating. We deposited Si onto the clean Ag(111) surface by holding it at 230 °C. By optimizing the sample preparation, we could obtain a surface predominantly covered by the (4×4) phase.

*jonoda@afm.k.u-tokyo.ac.jp

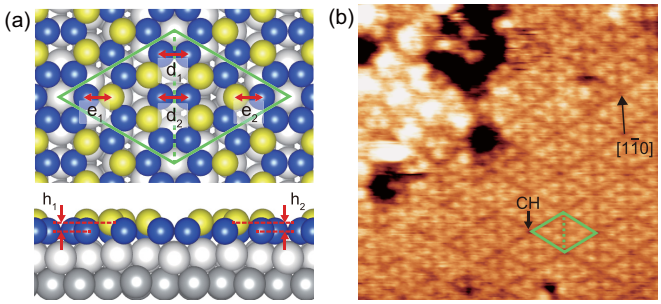

FIG. 1. Structural model and AFM topographic image of the (4×4) silicene on Ag(111) surface. (a) Structural model of the (4×4) unit cell determined by LEED [8]. Si(u) and Si(d) atoms are colored in yellow and blue, while first and second layer Ag atoms are painted with lighter and darker gray, respectively. (b) A typical AFM image (10×10 nm^2) of the (4×4) silicene on Ag(111) surface. The green rhombus represents the (4×4) unit cell. The acquisition parameters are the resonance frequency $(f_0) = 153.407$ kHz, the cantilever-oscillation amplitude $(A) = 168$ Å, the spring constant $(k) = 28.4$ N/m, the sample bias $(V_S) = 0$ mV, and $\Delta f = -10.0$ Hz.

Figure 1(a) shows the structural model of the (4×4) silicene on the Ag(111) surface determined by a tensor low-energy electron diffraction (LEED) analysis [8]. There are six upper-buckled Si [Si(u)] and 12 lower-buckled Si [Si(d)] atoms in the unit cell with slight height differences depending on their positions in the right or left triangle in Fig. 1(a). In previous STM and AFM studies, only the protruded Si(u) atoms were resolved, while the other Si(d) atoms were not. Figure 1(b) shows a typical AFM image of the (4×4) silicene formed on an Ag(111) substrate. Here, we observed the surface with the constant-frequency-shift (Δf) mode and the present AFM feedback regulation was working in the attractive force regime. The AFM image of the (4×4) phase represents six protrusions inside and the corner hollow (CH) site at the edge of the unit cell [green rhombus in Fig. 1(b)]. The observed feature is similar to those obtained by STM [2,3] and AFM [10,11].

As shown in Fig. 2(a), a closer look at the (4×4) phase shows a more detailed atomic structure. Surprisingly, not only the six Si(u) but also the 12 Si(d) atoms were able to be resolved by AFM. We found that some of the underlying Si(d) atoms in Fig. 2(a) form honeycomb rings surrounding CH, as shown in the (4×4) silicene model [Fig. 1(a)]. Henceforth, we refer to this imaging mode as the (4×4) mode. The reason why our AFM showed such high-resolution images could be that Si cantilevers have sharper apices in comparison with qPlus sensors [10,11], and also that the apices form reactive chemical bonds with surface Si atoms, as will be discussed. Moreover, during the AFM characterization of the (4×4) phase, we occasionally observed contrast changes. As shown in Fig. 2(b), when we scanned the area from the upper to lower with the (4×4) mode, the tip state suddenly changed [arrow in Fig. 2(b); the tip approached the surface by 0.6 Å in this particular case] and the AFM contrast switched from (4×4) to the honeycomb feature (referred to as the honeycomb mode). The AFM image of Fig. 2(c) showing the honeycomb mode represents more clearly the individual Si atoms of the (4×4)

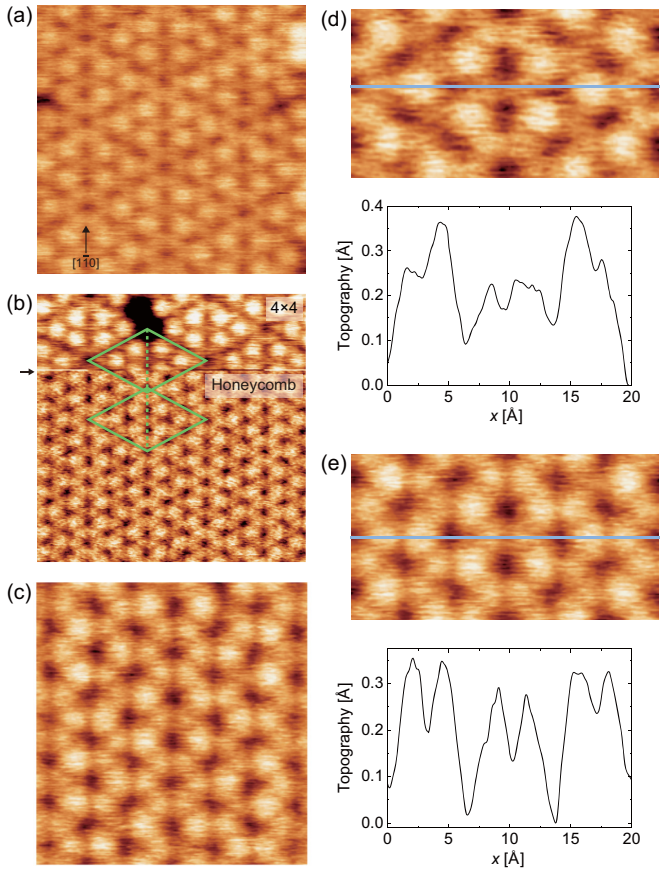

FIG. 2. High-resolution AFM images of the (4×4) silicene with different imaging modes. (a) (4×4) mode (3.5×3.6 nm^2, $f_0 = 158.348$ kHz, $A = 142$ Å, $k = 31.3$ N/m, $V_S = 0$ mV, and $\Delta f = -20.7$ Hz). (b) Transition from (4×4) to honeycomb modes (5×5 nm^2, $f_0 = 153.407$ kHz, $A = 168$ Å, $k = 28.4$ N/m, $V_S = 0$ mV, and $\Delta f = -15.2$ Hz). The green rhombuses represent the (4×4) unit cells under different modes. (c) Honeycomb mode (2.3×2.5 nm^2, $f_0 = 153.862$ kHz, $A = 152$ Å, $k = 28.4$ N/m, $V_S = 0$ mV, and $\Delta f = -56.1$ Hz). (d) and (e) show AFM images under (4×4) and honeycomb modes [cropped from (a) and (c)] and line profiles in the (4×4) unit cell, respectively.

silicene. It is well known that AFM topographic patterns can be changed by structural and chemical elements at the tip apex [34], even if we use the same Si cantilever. Thus, the difference between the (4×4) and honeycomb modes is derived from such a subtle modification at the tip apex.

Since it is important to know to what extent we can extract structural information quantitatively, we discuss the geometric values of the silicene on Ag(111) acquired by AFM. Figures 2(d) and 2(e) show line profiles in the unit cell in the (4×4) and honeycomb modes, respectively. It is obvious that height differences between Si(u) and Si(d) atoms are more distinct for the (4×4) contrast mode. Although the AFM topographic height is dependent on the set point of Δf [33], we attempt to statistically estimate the lateral and vertical displacements of the relevant Si atoms [see Fig. 1(a) for the definition] using AFM images in the (4×4) and honeycomb modes (see Sec. I of the Supplemental Material [35] for measurements of the structural parameters). A summary of

TABLE I. Structural parameters for (4 × 4) silicene on Ag(111).

	d_1 (Å)	d_2 (Å)	e_1 (Å)	e_2 (Å)	h_1 (Å)	h_2 (Å)
AFM [(4 × 4) mode]	2.2 ± 0.1	2.6 ± 0.1	2.5 ± 0.1	2.2 ± 0.2	0.15 ± 0.04	0.12 ± 0.02
AFM (honeycomb mode)	2.2 ± 0.1	2.2 ± 0.2	2.5 ± 0.1	2.41 ± 0.05	0.05 ± 0.02	0.04 ± 0.01
LEED [8]	2.31	2.29	2.17	2.17	0.77	0.74
RHEPD [36]					0.83 ± 0.05	
DFT [2]					0.75	
DFT [3]					0.7	
DFT [9]	2.30	2.34	2.17	2.18	0.77	0.76

the geometric values in each imaging mode is shown in Table I, which also includes those obtained by LEED [8], reflection high-energy positron diffraction (RHEPD) [36], and density functional theory (DFT) calculations [2,3,9].

In terms of the lateral displacements, d_1 and d_2 actually correspond to the bond length of Si(d)-Si(d) [see Fig. 1(a)]. We found that d_1 and d_2 in both imaging modes showed good agreement with those acquired by LEED (Table I). On the other hand, the values for the lateral displacements of e_1 and e_2 were systematically estimated at more than 2.4 Å. Taking into consideration that e_1 and e_2 are Si(u)-Si(d) bond lengths projected onto the surface plane, the values are clearly overestimated compared to those by LEED and DFT (Table I). Although we consider that some of the deviated values such as d_2 and e_2 in the (4 × 4) mode are derived from the asymmetry of the tip apex (see Table S1 in the Supplemental Material [35]), the tendency that e_1 and e_2 in both imaging modes showed larger values than those by LEED could be related to other factors.

We also found discrepancies in the values for vertical displacements. As shown in Table I, h_1 and h_2 in the (4 × 4) mode were estimated at about 0.14 Å. On the other hand, those for the honeycomb mode were almost one third of the values for the (4 × 4) mode, ∼0.05 Å. This is the reason why Si(u) and Si(d) atoms appear to be almost identical in this imaging mode. In either imaging mode, the vertical displacements between Si(u) and Si(d) atoms estimated by AFM are much smaller compared to those obtained by other experiments and calculations, i.e., 0.7–0.8 Å (see Table I). We will discuss the reasons for the discrepancies in the lateral and vertical displacements of Si(u)-Si(d).

To obtain more insight into the imaging mechanism of high-resolution AFM, we performed site-specific force spectroscopy on the surface. Figure 3(a) shows the measured distance dependences of the frequency shift [$\Delta f_{\mathrm{Total}}(z)$ curves] at S(u) and Si(d) under the (4 × 4) mode, as marked in the inset of Fig. 3(a). As depicted in Fig. S2(a) in the Supplemental Material [35], we deduced the background (BG) curve by analytically fitting the $\Delta f_{\mathrm{Total}}(z)$ curve acquired at the CH site, and then obtained short-range (SR) frequency shift [$\Delta f_{\mathrm{SR}}(z)$] curves [Fig. S2(b) in the Supplemental Material [35]]. Finally, the $\Delta f_{\mathrm{SR}}(z)$ curves were converted to $F_{\mathrm{SR}}(z)$ curves [Fig. 3(b)] using the inversion method [37]. In Fig. 3(b), we can see the magnitude of the maximum interaction forces of 1.0 nN on the Si(u) site and 0.9 nN on the Si(d) site, respectively. We also find that the maximum attractive forces can vary in the range of 1–2 nN depending on the tip state (not shown here). Such large attractive forces are comparable with those on Si adatom sites on the Si(111)-(7 × 7) surface [38–40], indicating the formation of chemical bonds between the tip and surface Si atoms [41,42]. Under the present experimental condition, it was found that AFM topographic images could be obtained with almost the maximum attractive force [Fig. 3(b)], which corresponds to the region where the magnitude of $\Delta f_{\mathrm{Total}}(z)$ steeply decreases [$0 < z < 1$ Å in Fig. 3(a)]. It is noteworthy that the $\Delta f_{\mathrm{Total}}(z)$ curves for Si(u) and Si(d) in a such region have slopes parallel to each other with a separation of 0.17 Å; thus the values of h_1 and h_2 could be almost independent from the set point of Δf. While Majzik *et al.* observed (4 × 4) silicene at the repulsive force regimes on Si atoms [11], we observed the atoms at the attractive force regimes, as did Resta *et al.* [10]. The present results are also comparable with the AFM observation using CO tips [28,29,31], where the Pauli repulsive force gives high-resolution images on flat 2D materials. We anticipate that high-resolution AFM by an attractive chemical force can be applied to many other buckled 2D materials.

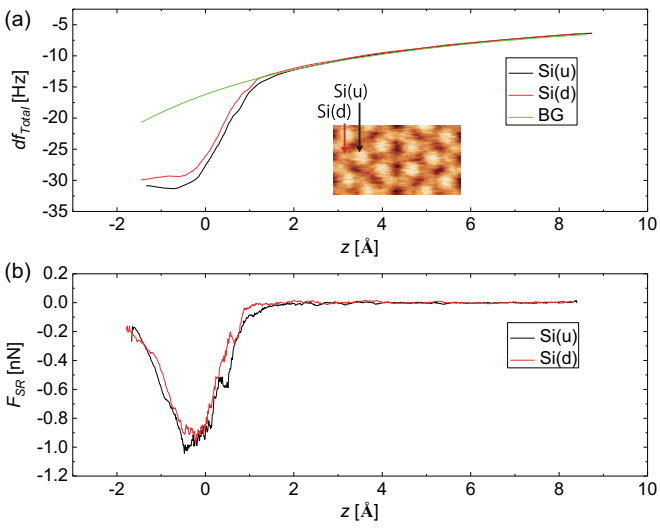

FIG. 3. Site-specific force spectroscopy. (a) Δf curves measured on Si(u) and Si(d) sites on the (4 × 4) silicene, as indicated in the inset. The background (BG) curve is also included for subtraction of the long-range components [see Fig. S2(a)]. (b) $F_{\mathrm{SR}}(z)$ curves on the Si(u) and Si(d) sites. The origin of z is adjusted to the point where Δf becomes the set point for AFM topographic images. The acquisition parameters are $f_0 = 158.348$ kHz, $A = 142$ Å, $k = 31.3$ N/m, and $V_S = 0$ mV.

One of the reasons for the discrepancy in the lateral and vertical displacements of Si(u)-Si(d) is considered to be the different mechanical responses on the Si(u) and Si(d) atoms toward the vertical direction. We can see such examples in previous AFM studies of buckled dimer atoms on a Si(100) surface [43–45]. With regard to the lateral displacements between the dimer atoms, experimentally obtained values became 2.9 Å [45] or 3.0 Å [43], which are larger than those found by LEED (about 2.28 Å) [46]. This was explained by the flipping of the dimer atoms induced by the AFM tip during scanning [43,45]. Similarly, while Si(u) atoms in the (4×4) silicene tend to maintain their original height during scanning, Si(d) atoms can be pulled up by the formation of a chemical bond with the tip, resulting in the larger lateral displacements of e_1 and e_2. Here, we can consider various tip-induced events accompanying the vertical pulling of Si(d) atoms, such as flipping or popping (see Sec. III in the Supplemental Material [35] for a discussion of the tip-induced events), though a theoretical calculation is necessary for further discussion. In any case, the tip-induced displacement of Si(d) atoms can cause hysteresis in the force curve in one oscillation cycle because after Si(d) atoms are pulled up in the approach path, they can be disconnected at a different vertical position in the retraction path. Such a nonconservative tip-surface interaction is detected as a dissipation signal in AFM [34,47,48]. As shown in Fig. S4 in the Supplemental Material [35], we actually observed dissipation signals only at the Si(d) atom sites with particular tip states. According to the transition state theory taking into account the soft mode caused by the tip and the bistable potential energy surface [49], a force curve under a nonconservative interaction at finite temperature can be a kind of an average of the approach and retraction curves. Thus, AFM topographic images would have errors at the relevant sites. We could see the effects of bistability on AFM topography also in the studies of buckled dimer atoms. While the height of the buckled dimer atoms was experimentally evaluated as 0.73 ± 0.06 Å by LEED [46], it was demonstrated that the apparent height between the higher and lower dimer atoms could become about 0.1 Å in the AFM topography simulation at intermediate temperatures (70–200 K) [44]. Therefore, provided a similar situation occurs on the (4×4) silicene on an Ag(111) surface at RT, it is reasonable to observe apparently small vertical displacements of h_1 and h_2 by AFM (Table I). Moreover, based on this concept, we can ascribe even the difference between the (4×4) and honeycomb imaging modes to different mechanical responses at the tip apex side, since the shape of the hysteresis in the force curve strongly depends on the tip apex structures [50]. Note that the formation of a chemical bond at an Si(d) site suggests a weakening of Si(d)-Ag interactions at the interface, thus such relaxations of the surface and/or tip atoms could be keys to high-resolution AFM.

Another origin of the discrepancy in h_1 and h_2 obtained by AFM and LEED is the different degrees of propagation of the dangling bonds out of Si(u) and Si(d) toward the vertical direction. In this case, the directionality of the dangling bonds of Si(u) and Si(d) atoms [see Fig. 6(a) in Ref. [51]] could also play some role in the elongation of the lateral displacement of e_1 and e_2, as discussed in Ref. [43]. To elucidate the origin of the discrepancy in the lateral and vertical displacements between AFM and other techniques, further theoretical considerations such as force curves based on first-principles calculations including the tip are necessary.

In summary, we show that AFM can resolve not only Si(u) but also Si(d) atoms on a (4×4) silicene/Ag(111) surface. We find there are two types of imaging modes representing (4×4) and honeycomb features, respectively, depending on the AFM tip state. Both imaging modes allow us to discuss the geometric structure of the (4×4) silicene. Site-specific force spectroscopy revealed that the high resolution of the AFM images originates from the formation of chemical bonds between the apex and surface Si atoms. Using the analogy of buckled dimer atoms on the Si(100) surface, we succeed in qualitatively interpreting the discrepancy in the lateral and vertical displacements of Si(u)-Si(d) evaluated by AFM and LEED. The suggested weakening of Si(d)-Ag interactions induced by tip pulling gives us the perspective that measurements of the dissipation signals at the atomic scale will extend our knowledge of the exfoliation of silicene from its metal substrates. Such examples can be found in studies of graphene on different substrates (graphite [52] and Pt [30]), where individual C atoms are positioned on inequivalent surface sites. Although features of the detailed AFM imaging mechanisms remain to be solved theoretically, the ability to observe underlying Si(d) atoms—and thus all constituent Si atoms in silicene—will be useful for determining not only the atomic structures of silicene in other phases, but also the edge and defect structures, intriguing Si derivatives such as pentagonal Si nanoribbons [53], or other emerging 2D materials.

The authors thank K. Kawahara and C.-L. Lin for valuable discussions, and A. Shiotari and N. Kawakami for technical support. This work was supported by Grants-in-Aid for JSPS Fellows (14J00689) and for Scientific Research (15H03566, 16H00933, 16H00959, 16K13680, 16K17482) from the Ministry of Education, Culture, Sports, Science, and Technology of Japan (MEXT). We also acknowledge financial support from the Asahi Glass Foundation, the Mitsubishi Foundation, the Yamada Science Foundation, and the Ube Foundation.

[1] C.-C. Liu, W. Feng, and Y. Yao, Phys. Rev. Lett. **107**, 076802 (2011).

[2] P. Vogt, P. De Padova, C. Quaresima, J. Avila, E. Frantzeskakis, M. C. Asensio, A. Resta, B. Ealet, and G. Le Lay, Phys. Rev. Lett. **108**, 155501 (2012).

[3] C.-L. Lin, R. Arafune, K. Kawahara, N. Tsukahara, E. Minamitani, Y. Kim, N. Takagi, and M. Kawai, Appl. Phys. Express **5**, 045802 (2012).

[4] B. Feng, Z. Ding, S. Meng, Y. Yao, X. He, P. Cheng, L. Chen, and K. Wu, Nano Lett. **12**, 3507 (2012).

[5] H. Jamgotchian, Y. Colignon, N. Hamzaoui, B. Ealet, J. Hoarau, B. Aufray, and J. Bibérian, J. Phys.: Condens. Matter **24**, 172001 (2012).
[6] D. Chiappe, C. Grazianetti, G. Tallarida, M. Fanciulli, and A. Molle, Adv. Mater. **24**, 5088 (2012).
[7] H. Enriquez, S. Vizzini, A. Kara, B. Lalmi, and H. Oughaddou, J. Phys.: Condens. Matter **24**, 314211 (2012).
[8] K. Kawahara, T. Shirasawa, R. Arafune, C.-L. Lin, T. Takahashi, M. Kawai, and N. Takagi, Surf. Sci. **623**, 25 (2014).
[9] A. Curcella, R. Bernard, Y. Borensztein, A. Resta, M. Lazzeri, and G. Prévot, Phys. Rev. B **94**, 165438 (2016).
[10] A. Resta, T. Leoni, C. Barth, A. Ranguis, C. Becker, T. Bruhn, P. Vogt, and G. Le Lay, Sci. Rep. **3**, 2399 (2013).
[11] Z. Majzik, M. R. Tchalala, M. Švec, P. Hapala, H. Enriquez, A. Kara, A. J. Mayne, G. Dujardin, P. Jelínek, and H. Oughaddou, J. Phys.: Condens. Matter **25**, 225301 (2013).
[12] Z.-L. Liu, M.-X. Wang, J.-P. Xu, J.-F. Ge, G. Le Lay, P. Vogt, D. Qian, C.-L. Gao, C. Liu, and J.-F. Jia, New J. Phys. **16**, 075006 (2014).
[13] C. Grazianetti, D. Chiappe, E. Cinquanta, G. Tallarida, M. Fanciulli, and A. Molle, Appl. Surf. Sci. **291**, 109 (2014).
[14] M. R. Tchalala, H. Enriquez, H. Yildirim, A. Kara, A. J. Mayne, G. Dujardin, M. A. Ali, and H. Oughaddou, Appl. Surf. Sci. **303**, 61 (2014).
[15] J. Zhuang, X. Xu, Y. Du, K. Wu, L. Chen, W. Hao, J. Wang, W. K. Yeoh, X. Wang, and S. X. Dou, Phys. Rev. B **91**, 161409 (2015).
[16] C. Grazianetti, D. Chiappe, E. Cinquanta, M. Fanciulli, and A. Molle, J. Phys.: Condens. Matter **27**, 255005 (2015).
[17] J. Sone, T. Yamagami, Y. Aoki, K. Nakatsuji, and H. Hirayama, New J. Phys. **16**, 095004 (2014).
[18] E. Cinquanta, E. Scalise, D. Chiappe, C. Grazianetti, B. van den Broek, M. Houssa, M. Fanciulli, and A. Molle, J. Phys. Chem. C **117**, 16719 (2013).
[19] H. Enriquez, A. Kara, A. J. Mayne, G. Dujardin, H. Jamgotchian, B. Aufray, and H. Oughaddou, J. Phys.: Conf. Ser. **491**, 012004 (2014).
[20] H. Jamgotchian, B. Ealet, Y. Colignon, H. Maradj, J. Hoarau, J. Biberian, and B. Aufray, J. Phys.: Condens. Matter **27**, 395002 (2015).
[21] W. Wang, W. Olovsson, and R. I. G. Uhrberg, Phys. Rev. B **92**, 205427 (2015).
[22] G. Prévôt, R. Bernard, H. Cruguel, and Y. Borensztein, Appl. Phys. Lett. **105**, 213106 (2014).
[23] E. Salomon, R. El Ajjouri, G. Le Lay, and T. Angot, J. Phys.: Condens. Matter **26**, 185003 (2014).
[24] H. Fu, L. Chen, J. Chen, J. Qiu, Z. Ding, J. Zhang, K. Wu, H. Li, and S. Meng, Nanoscale **7**, 15880 (2015).
[25] P. Lagarde, M. Chorro, D. Roy, and N. Trcera, J. Phys.: Condens. Matter **28**, 075002 (2016).
[26] C.-L. Lin, R. Arafune, K. Kawahara, M. Kanno, N. Tsukahara, E. Minamitani, Y. Kim, M. Kawai, and N. Takagi, Phys. Rev. Lett. **110**, 076801 (2013).
[27] Y. Feng, D. Liu, B. Feng, X. Liu, L. Zhao, Z. Xie, Y. Liu, A. Liang, C. Hu, Y. Hu *et al.*, Proc. Natl. Acad. Sci. USA **113**, 14656 (2016).
[28] L. Gross, F. Mohn, N. Moll, P. Liljeroth, and G. Meyer, Science **325**, 1110 (2009).
[29] M. P. Boneschanscher, J. Van Der Lit, Z. Sun, I. Swart, P. Liljeroth, and D. Vanmaekelbergh, ACS Nano **6**, 10216 (2012).
[30] B. de la Torre, M. Ellner, P. Pou, N. Nicoara, R. Pérez, and J. M. Gómez-Rodríguez, Phys. Rev. Lett. **116**, 245502 (2016).
[31] S. Barja, S. Wickenburg, Z.-F. Liu, Y. Zhang, H. Ryu, M. M. Ugeda, Z. Hussain, Z.-X. Shen, S.-K. Mo, E. Wong *et al.*, Nat. Phys. **12**, 751 (2016).
[32] M. Schwarz, A. Riss, M. Garnica, J. Ducke, P. S. Deimel, D. A. Duncan, P. K. Thakur, T.-L. Lee, A. P. Seitsonen, J. V. Barth *et al.*, ACS Nano **11**, 9151 (2017).
[33] Y. Sugimoto, P. Pou, Ó. Custance, P. Jelinek, S. Morita, R. Pérez, and M. Abe, Phys. Rev. B **73**, 205329 (2006).
[34] N. Oyabu, P. Pou, Y. Sugimoto, P. Jelinek, M. Abe, S. Morita, R. Pérez, and O. Custance, Phys. Rev. Lett. **96**, 106101 (2006).
[35] See Supplemental Material at http://link.aps.org/supplemental/10.1103/PhysRevB.96.241302 for measurements of the structural parameters, evaluation of the BG curve in force spectroscopy, discussion of the tip-induced events, and dissipation in AFM observations.
[36] Y. Fukaya, I. Mochizuki, M. Maekawa, K. Wada, T. Hyodo, I. Matsuda, and A. Kawasuso, Phys. Rev. B **88**, 205413 (2013).
[37] J. E. Sader and S. P. Jarvis, Appl. Phys. Lett. **84**, 1801 (2004).
[38] Y. Sugimoto, P. Pou, M. Abe, P. Jelinek, R. Pérez, S. Morita, and O. Custance, Nature (London) **446**, 64 (2007).
[39] J. Onoda, K. Niki, and Y. Sugimoto, Phys. Rev. B **92**, 155309 (2015).
[40] J. Onoda, M. Ondráček, P. Jelínek, and Y. Sugimoto, Nat. Commun. **8**, 15155 (2017).
[41] R. Pérez, M. C. Payne, I. Štich, and K. Terakura, Phys. Rev. Lett. **78**, 678 (1997).
[42] M. Lantz, H. Hug, R. Hoffmann, P. Van Schendel, P. Kappenberger, S. Martin, A. Baratoff, and H.-J. Güntherodt, Science **291**, 2580 (2001).
[43] Y. J. Li, H. Nomura, N. Ozaki, Y. Naitoh, M. Kageshima, Y. Sugawara, C. Hobbs, and L. Kantorovich, Phys. Rev. Lett. **96**, 106104 (2006).
[44] L. Kantorovich and C. Hobbs, Phys. Rev. B **73**, 245420 (2006).
[45] D. Sawada, T. Namikawa, M. Hiragaki, Y. Sugimoto, M. Abe, and S. Morita, Jpn. J. Appl. Phys. **47**, 6085 (2008).
[46] S. Mizuno, T. Shirasawa, Y. Shiraishi, and H. Tochihara, Phys. Rev. B **69**, 241306(R) (2004).
[47] A. Sweetman, S. Jarvis, R. Danza, J. Bamidele, S. Gangopadhyay, G. A. Shaw, L. Kantorovich, and P. Moriarty, Phys. Rev. Lett. **106**, 136101 (2011).
[48] S. Jarvis, A. Sweetman, J. Bamidele, L. Kantorovich, and P. Moriarty, Phys. Rev. B **85**, 235305 (2012).
[49] L. N. Kantorovich and T. Trevethan, Phys. Rev. Lett. **93**, 236102 (2004).
[50] S. P. Jarvis, L. Kantorovich, and P. Moriarty, Beilstein J. Nanotechnol. **4**, 941 (2013).
[51] Z.-X. Guo, S. Furuya, J.-i. Iwata, and A. Oshiyama, Phys. Rev. B **87**, 235435 (2013).
[52] S. Kawai and H. Kawakatsu, Phys. Rev. B **79**, 115440 (2009).
[53] J. I. Cerdá, J. Sławińska, G. Le Lay, A. C. Marele, J. M. Gómez-Rodríguez, and M. E. Dávila, Nat. Commun. **7**, 13076 (2016).